Systematic time-coarse-graining for driven quantum systems

Leon Bello,[*,†] Wentao Fan,[†,‡] Aditya Gandotra, and Hakan E. Türeci
Department of Electrical and Computer Engineering, Princeton University, Princeton, New Jersey, USA

(Received 8 July 2024; revised 11 December 2024; accepted 22 April 2025; published 15 May 2025)

Real-world experiments on quantum systems are always performed with measurement apparatus whose interaction times with the systems are finite. This restricts the observable quantum states to the space of time-coarse-grained density matrices $\{\overline{\rho}(t)\}$, providing motivation for the time-coarse-graining (TCG) approach that solves for $\overline{\rho}(t)$ without ever referring to the unobservable $\rho(t)$ of infinite time resolution. Phenomenologically, this implies that coherent transitions far outside the bandwidth would be filtered out, leaving only their effective impacts on the "slow" dynamics resolvable by the finite time resolution of the measurements. Therefore, the TCG framework provides rigorous justification for many existing effective Hamiltonian methods in the literature that aim at capturing the unitary part of the long-time dynamics. However, since time-coarse-graining is fundamentally irreversible, the resulting effective model allows for secular loss of information and dissipation of energy in general, which cannot be captured by any unitary effective models and has to be treated with explicit time-coarse-graining. Such incoherent effects are particularly prominent in driven nonlinear quantum systems where exchange of information and energy with the drive gives rise to incoherent effective dynamics at all finite time resolutions in general. While rigorous in principle, existing TCG methods in the literature can be applied only to simple systems by one iteratively solving superoperator equations at low orders in the coupling strengths. The complexity of such methods prevents systematic study of the time-coarse-grained dynamics and limits analytical results to the IR (low-resolution) limit in most cases. We address these limitations in this paper, presenting a systematic time-coarse-graining method that overcomes the complexities and restrictions of current techniques, offering a comprehensive and accurate modeling framework for driven nonlinear quantum systems. We derive closed-form formulas as well as diagrammatic representations for both unitary and nonunitary contributions, in the form of an effective Hamiltonian and nonunitary dissipators at arbitrary order in the coupling strengths, and complement this with a computer-algebra software package. We demonstrate the effectiveness of the method using several typical models of driven nonlinear systems in superconducting circuits, and show that it generalizes and improves on existing methods by providing more accurate results and explaining phenomena that have not been accounted for.

DOI: 10.1103/PhysRevApplied.23.054042

I. INTRODUCTION

When a measurement apparatus interacts with the electromagnetic fields emanating from a quantum system, its output is *always* a coarse-grained function of exact physical variables at precise moments in time and/or precise locations in space. Therefore, the *observable dynamics* in any quantum system depends on the time and/or spatial resolution of the measuring apparatus. For typical quantum optical systems, the most important coarse-graining scale is the time resolution of the measuring device, which is limited by its bandwidth (see, e.g., Appendix D in Ref. [1]). Although not always explicitly acknowledged, the measurement time resolution is a particularly crucial free parameter for driven nonlinear quantum systems, since the exchange of information and energy with an external drive can have long-lasting effects on the system that propagate through different timescales and manifest themselves in different forms due to nonlinearities. In many situations, the finite time resolution of the measurement apparatus can be captured by one working with the time-coarse-grained density matrix $\overline{\rho}(t)$ of the measured system, as illustrated in Fig. 1:

$$\overline{\rho}(t) = \int_{-\infty}^{\infty} \tilde{f}_\tau(t-t')\rho(t')\,dt', \tag{1}$$

where $\tilde{f}_\tau(t)$ is a moving-average function with width τ that we call the "coarse-graining timescale."

This issue of modeling the observable behavior in multiscale systems provides motivation for the time-coarse-graining (TCG) approach, which aims to directly capture

[*]Contact author: lbello@princeton.edu
[†]These authors contributed equally to this work.
[‡]Contact author: wentaof@princeton.edu

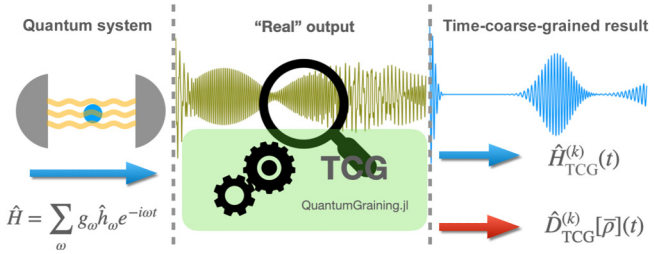

FIG. 1. Illustration of the inherent time-coarse-graining happening during a measurement. A quantum system produces a high-bandwidth signal. This signal drives a measurement apparatus that is band-limited, producing a time-coarse-grained version of the real dynamics. The TCG method aims to produce a direct description of the time-coarse-grained observables, which can be captured by an effective quantum master equation for the coarse-grained density matrix $\overline{\rho}$ in the appropriate rotating frame determined by the central frequency of the measuring device.

the observable, time-coarse-grained dynamics with no reference to unresolvable degrees of freedom at any step. In the TCG framework [2], the time-coarse-grained dynamics of the system is described by an effective quantum master equation, despite the microscopic dynamics being fully unitary. This approach has both fundamental and practical value. Fundamentally, it reflects the fact that all physical apparatus have a finite response time and inevitably perform some type of time-coarse-graining of information during their interactions with the measured systems. Practically, it can also offer significant simplification of the effective model by separating the experimentally relevant observables from the unresolvable ones, while at the same time keeping track of the latter's impact on the former. This feature is becoming increasingly important as recent advancements in quantum devices have focused on precise engineering of effective interactions via parametric driving, which often involves regimes where counterrotating processes, typically regarded as negligible, assume significance, rendering the commonly used rotating-wave approximation (RWA) or even more sophisticated effective Hamiltonian methods, unsatisfactory [3–5].

The TCG method offers an alternative approach for modeling such multitimescale systems, but so far the TCG methods in the literature can be applied perturbatively only to simple systems at very low orders in the coupling strengths. Furthermore, existing analyses either assume some particular coarse-graining window function or work in the IR limit and ignore all possible dependencies on the shape or width of the window function.

In this work, we significantly improve the TCG method and present a fully systematic solution to the time-coarse-graining approach. We introduce the systematic time-coarse-graining (STCG) method, which gives a closed-form solution to arbitrary orders for general driven quantum systems, and for arbitrary coarse-graining window functions. Our approach explicitly derives a Liouvillian for $\overline{\rho}(t)$, without having to solve for the exact dynamics or assume any knowledge of the initial density matrix ρ with infinite time resolution. Unlike previous attempts at deriving the TCG Liouvillian, our method is completely general, with closed-form formulas for the contributions to any order in the expansion. In addition, we also introduce a diagrammatic representation of the resulting TCG superoperators that can not only function as a bookkeeping tool for the quantum Liouvillian at each order but can also provide intuitive guidance for designing the microscopic interactions and drives to achieve certain effective long-time dynamics.

In addition to its conceptual novelty, our approach also has important numerical advantages. Indeed, numerically solving the time evolution of a driven nonlinear quantum system with much higher time resolution than the measured variable dynamics can be very inefficient and often unfeasible, as the dynamics of the system encompass vastly different timescales, making the equations very stiff and numerically unstable; to make the situation worse, the solutions obtained in such brute-force approaches are usually difficult to interpret. Our method, STCG, gives an effective low-frequency quantum model leveraging the separation of timescales as small parameters in a systematic expansion, giving an effective low-frequency description of the dynamics, which is long-time stable and efficient to study numerically. Furthermore, to lower the barrier to entry for the STCG method, we have developed a JULIA package, QuantumGraining.jl, that automates STCG to any order, generating both the effective Hamiltonian terms obtainable through existing methods and additional nonunitary corrections.

This paper is organized as follows: We begin with a canonical example, the Rabi model, illustrating the conceptual and mechanistic elements behind the TCG method in Sec. II. We then delve into the theoretical background in Sec. III, where we introduce the STCG method in the context of other methods, presenting the essential concepts of the theory, while reserving the detailed derivation to Supplemental Material [6]. In Sec. IV, we introduce a diagrammatic approach for deriving the TCG master equation. In Sec. V, we showcase the method using two additional examples—(1) the Kerr parametron and (2) the driven Duffing oscillator. In particular, we show that the TCG method predicts measurable modifications to the dynamics of these models, some of which are supported by analytical or numerical results in the literature obtained by other methods. Finally, we present our conclusions and discuss future prospects in Sec. VI. In Supplemental Material [6], we introduce QuantumGraining.jl, a JULIA package that automates the TCG procedure, together with a short code example for the Rabi model. In other work [7], we use this tool to analyze in detail the measurement problem.

II. AN ILLUSTRATIVE EXAMPLE: THE TIME-COARSE-GRAINED RABI MODEL

To demonstrate our method, we start with a simple but illustrative example—the Rabi model. The Rabi model describes the interaction between a single linear cavity mode and an atom described by a two-level system (TLS), and can be simplified to the Jaynes-Cummings model when the RWA is justified. In the so-called ultrastrong-coupling regime, the Rabi model is of special interest since the RWA breaks down when the spin-cavity coupling strength becomes comparableto or greater than the mode frequencies [8–10], and special approaches that go beyond the RWA are required [11–13].

More concretely, the model we consider here is described by the following Hamiltonian terms in the interaction picture:

$$\hat{H} = \frac{g}{2}\left(\hat{a}^\dagger\hat{\sigma}_+ e^{+i(\omega_c+\omega_a)t} + \hat{a}\hat{\sigma}_- e^{-i(\omega_c+\omega_a)t}\right) + \frac{g}{2}\left(\hat{a}^\dagger\hat{\sigma_-} e^{+i(\omega_c-\omega_a)t} + \hat{a}\hat{\sigma}_+ e^{-i(\omega_c-\omega_a)t}\right), \quad (2)$$

where ω_c (ω_a) is the cavity (atom) resonance.

To showcase the time-coarse-graining method, we focus on this ultrastrong-coupling regime where the coupling strength g is comparable to the TLS and cavity frequencies ω_a and ω_c. i.e., $g \approx \omega_c$ ($g \approx \omega_a$). In that regime, the counterrotating terms assume significance, and the induced dynamics depend on the time resolution of the measurement apparatus. The numerical simulations reported in this section assume the following set of parameters:

$$\frac{\omega_c}{2\pi} = \frac{\omega_a}{2\pi} = 2\,\text{GHz}, \quad \frac{g}{2\pi} = 0.4\,\text{GHz}. \quad (3)$$

Under this set of parameters, the two-level population displays rapid oscillations whose envelope undergoes intricate evolution over a much longer timescale, as shown in Fig. 2. When the dynamics of a coherent-state cavity mode interacts with a single TLS, the Jaynes-Cummings model shows collapse-revival dynamics due to the photon-number dispersion of a coherent state. Interestingly, we show that these collapse-revival cycles are completely absent in the full Rabi-model dynamics (if all timescales can be resolved), and appear only under finite time resolution. The latter is directly captured by the STCG approach, as discussed below.

Using the STCG method, we obtain an effective description that gives us **directly** the time-averaged observables that would be obtained from a bandwidth-limited measurement apparatus, and we do not need to assume any knowledge of the density matrix $\rho(t)$ at an infinitely precise moment in time. The STCG prescription produces a set of Hamiltonian corrections, comprising products of the original Hamiltonian operators $\hat{s}_{\vec{\mu}} = \prod_{\mu_i\in\vec{\mu}} \hat{h}_{\mu_i}$ (i.e., multibody transitions or multimode resonances), and their corresponding coupling strengths $q_{\vec{\mu}}$.

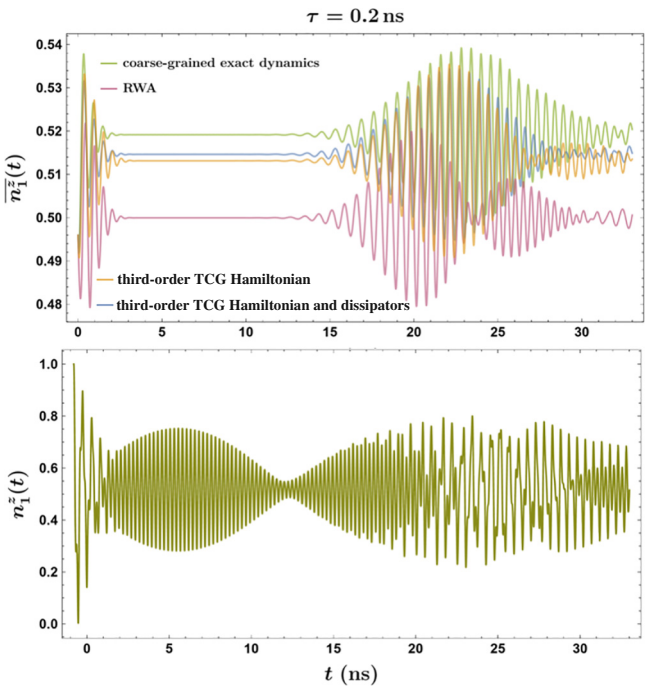

FIG. 2. Bottom: Numerical simulation of the excited TLS-state population $n_1^z(t)$, obtained by our numerically solving the Schrödinger equations for the interaction-picture Rabi Hamiltonian in Eq. (2). The initial state at $t_i = -0.8$ ns is $|1\rangle_s|\alpha = 4.5\rangle_c$, with $|1\rangle$ and $|\alpha = 4.5\rangle_c$ representing the exited TLS state and the coherent cavity state with amplitude $\alpha = 4.5$, respectively. All TCG simulations are performed without our making any further approximation of the perturbative TCG master equation. Top: Numerical simulation of the time-coarse-grained excited TLS-state population $\overline{n_1^z}(t)$ with a coarse-graining timescale τ of 0.2 ns. The coarse-grained exact dynamics is obtained by our directly applying the Gaussian averaging function $\tilde{f}_\tau(t)$ to the exact $n_1^z(t)$ in the bottom figure, whereas the TCG results are obtained by our numerically solving the corresponding TCG master equations. In all calculations the cavity Hilbert space is truncated to include the lowest 100 levels during the simulation. The initial state of all equations is taken to be the same.

Importantly, the time-coarse-grained evolution is not unitary in general, and the TCG effective Hamiltonian has to be complemented with a set of pairs of operators $(\hat{L}_{\vec{\mu}}, \hat{J}_{\vec{\nu}})$ with (generally) complex coefficients $\gamma^{(k)}_{\vec{\mu},\vec{\nu}}$ such that the time evolution of $\overline{\rho}(t)$ is given by the TCG master equation:

$$\partial_t\overline{\rho}(t) = -\left[\hat{H}_{\text{TCG}}(t), \overline{\rho}(t)\right] + \hat{D}_{\text{TCG}}(t)\overline{\rho}(t) = -\left[\sum_{k=1}^{\infty}\hat{H}^{(k)}_{\text{TCG}}(t), \overline{\rho}(t)\right] + \sum_{k=1}^{\infty}\hat{D}^{(k)}_{\text{TCG}}(t)\overline{\rho}(t), \quad (4)$$

$$\hat{H}_{\text{TCG(k)}} = q^{(k)}_{\vec{\mu}} e^{-i\left(\sum_j \mu_j\right)t}\prod_{\mu_i} h^{(k)}_{\mu_i}, \quad (5a)$$

$$\hat{D}^{(k)}_{\mathrm{TCG}}(t)\overline{\rho} = \gamma^{(k)}_{\vec{\mu},\vec{\nu}}\mathcal{D}\left[\hat{L}_{\vec{\mu}},\hat{J}_{\vec{\nu}}\right]e^{-i\left(\sum_{j_1}\mu_{j_1}+\sum_{j_2}\nu_{j_2}\right)t}. \quad (5b)$$

In the expressions above, $k = l + r$ is the order of the perturbative expansion in the original coupling strengths, and the (pseudo)dissipator notation $\mathcal{D}[\cdot,\cdot]$ is defined such that

$$\mathcal{D}\left[\hat{L}_{\vec{\mu}},\hat{J}_{\vec{\nu}}\right]\overline{\rho} \equiv \hat{L}_{\vec{\mu}}\overline{\rho}\hat{J}_{\vec{\nu}} - \frac{1}{2}\left\{\hat{J}_{\vec{\nu}}\hat{L}_{\vec{\mu}},\overline{\rho}\right\}. \quad (6)$$

These additional, nonunitary corrections are important, and are completely ignored by effective Hamiltonian methods, such as the Lie perturbation theory method [14].

We explain details of the calculation in the following sections, but for now we simply assume that the TCG effective Hamiltonian and effective (pseudo)dissipators can be perturbatively calculated as functions of the coarse-graining timescale τ and the original Hamiltonian, either manually or automatically using a computer-algebra system, such as the symbolic software package QuantumGraining.jl we developed. The full explicit calculation up to second order is shown in Supplemental Material [6].

To effectively capture the coarse-grained dynamics of the Rabi model, we apply the STCG perturbation theory up to the third order and derive the corresponding master equation. In particular, we see that the TCG procedure reproduces the RWA Hamiltonian at the first order (under the assumption of a simple filter function), and goes beyond it starting at the second order. For example, in the weak-coupling limit, realistic values of the coarse-graining timescale τ usually fall in the range $1/\omega_a \ll \tau \ll (1/|\omega_c - \omega_a|), 2/g$, and the most significant terms in the effective Hamiltonian are found to be as follows:

$$\hat{H}^{(2)}_{\mathrm{TCG}} \approx \hat{H}_{\mathrm{RWA}} + \frac{g^2}{8}\left[\frac{1}{2\omega_a} - \left(\tau^2 + \frac{1}{4\omega_a^2}\right)(\omega_a - \omega_c)\right] \times (1 + 2\hat{a}^\dagger\hat{a})\hat{\sigma}_z. \quad (7)$$

To first order, we get exactly the RWA Hamiltonian

$$\hat{H}_{\mathrm{RWA}} = \frac{g}{2}e^{-((\omega_a-\omega_c)^2\tau^2/2)}\left(e^{i(\omega_a-\omega_c)t}\hat{a}\hat{\sigma}_+ + e^{-i(\omega_a-\omega_c)t}\hat{a}^\dagger\hat{\sigma}_-\right) \approx \frac{g}{2}\left(e^{+i(\omega_a-\omega_c)t}\hat{a}\hat{\sigma}_+ + e^{-i(\omega_a-\omega_c)t}\hat{a}^\dagger\hat{\sigma}_-\right). \quad (8)$$

The filter-dependent factor $e^{-((\omega_a-\omega_c)^2\tau^2/2)}$ in the first line is a major difference from the standard RWA. Unlike the RWA, we consider the coarse-graining timescale τ as an experimentally tunable parameter, and the result is subject to significant modification over the RWA results once τ is large enough to be comparable to $1/|\omega_a - \omega_c|$. In general, as the coupling strength g approaches the ultrastrong-coupling regime or when the time resolution τ^{-1} becomes comparable with the detuning $|\omega_a - \omega_c|$, one needs to go beyond the simple expression in Eq. (8) and consider contributions from higher-order terms. Considering such a situation, we present the exact form of the Hamiltonian and (pseudo)dissipator corrections calculated with the QuantumGraining.jl package in Supplemental Material [6].

As mentioned, an important property of the STCG method is that it also captures the effective nonunitary dynamics of the system induced by the time-averaging. For example, at the second order, we get the following set of pseudodissipators in addition to the dispersive correction in the Hamiltonian:

$$\hat{L}_1 = \hat{J}_1 = \hat{a}\hat{\sigma}_+, \quad \gamma_1 = -i\frac{g^2\tau^2}{2}(\omega_c - \omega_a)e^{-2i(\omega_c-\omega_a)t}, \quad (9a)$$

$$\hat{L}_2 = \hat{J}_2 = \hat{a}^\dagger\hat{\sigma}_-, \quad \gamma_2 = i\frac{g^2\tau^2}{2}(\omega_c - \omega_a)e^{2i(\omega_c-\omega_a)t}. \quad (9b)$$

Notice that the coefficients γ_1 and γ_2 are purely imaginary, so the corresponding pseudodissipators do not break the time-reversal symmetry (hence the prefix "pseudo"). In addition, we do not expect significant secular effects from the second-order pseudodissipators since their coefficients are oscillatory at frequency $\pm 2(\omega_c - \omega_a)$ and vanish in the resonant limit when $\omega_c \to \omega_a$. In particular, they do not induce any secular gain or loss of the system energy, but rather only add small fluctuating corrections to the entropy and energy of the system.

However, this is not the case for higher-order corrections in general. For example, we have the following third-order contributions in the resonant limit where $\omega_c \to \omega_a$:

$$\hat{H}^{(3)}_{\mathrm{TCG}} \approx \lim_{\omega_c\to\omega_a}\hat{H}^{(2)}_{\mathrm{TCG}} - \frac{g^3}{32\omega_a^2}\hat{a}^\dagger\hat{a}\hat{a}^\dagger\hat{\sigma}_- + \mathrm{H.c.}, \quad (10)$$

$$\hat{D}^{(3)}_{\mathrm{TCG}} \approx \frac{ig^3}{32\omega_a^2}\left(\mathcal{D}[\hat{a}^2\hat{\sigma}_z,\hat{a}^\dagger\hat{\sigma}_+] - \mathcal{D}[\hat{a}^{\dagger 2}\hat{\sigma}_z,\hat{a}\hat{\sigma}_-]\right) + \mathrm{H.c.}, \quad (11)$$

from which we see that the unitary and nonunitary contributions both give rise to time-independent corrections to the Jaynes-Cummings model in the resonant limit. From the numerical simulation in Fig. 2 (obtained with a coarse-graining timescale τ of 0.2 ns), we see that they both have secular effects on the collapse and revival of the TLS population. In particular, although $\hat{D}^{(3)}_{\mathrm{TCG}}$ does not cause any dissipation of energy over long periods due to its purely imaginary prefactor, it does have observable secular effects on the *coherence* of the TLS, which affects the collapse-revival pattern of the TLS-state population. For example, the RWA (first-order TCG) and the third-order TCG Hamiltonians both make the false prediction of a double-revival pattern between $t = 15$ ns and $t = 35$ ns, which is removed by inclusion of the third-order pseudodissipators in $\hat{D}^{(3)}_{\mathrm{TCG}}$. As expected, inclusion of the pseudodissipators brings the TCG dynamics closer to the exact dynamics,

as can be observed in Fig. 2. The TCG master equations can be numerically simulated with much larger time steps without one encountering any stiffness problems compared with the exact von Neumann equation, which contains fast-oscillating counterrotating terms. Therefore, the TCG master equation not only offers analytical insights into the physics of an interacting system but also allows much more efficient numerical simulation of the dynamics.

III. EFFECTIVE STATIC METHODS AND TIME-COARSE-GRAINING

In this work, we focus on time-coarse-graining Hamiltonian dynamics, i.e., closed-system dynamics fully described by a Hamiltonian. In Ref. [7], we delve into the more general problem of time-coarse-graining an open quantum system. In general terms, we consider interaction-picture Hamiltonians $\hat{H}$ of the form

$$\hat{H} = \sum_{\omega\in\Omega} g_\omega \hat{h}_\omega e^{-i\omega t}, \tag{12}$$

where Ω is the set of all the frequencies appearing in the Hamiltonian. The frequencies involved can be of vastly different scales, and we would like to obtain an effective, low-bandwidth description of the resulting dynamics. For example, the RWA corresponds to one simply removing all Hamiltonian terms $\hat{h}_\omega$ with "fast" frequencies from the sum, and retaining those with "slow" frequencies.

In the literature, the problem of fast-varying time-dependent Hamiltonians is treated with a variety of tools, as illustrated by the Venn diagram in Fig. 3. Some of these methods rely directly on one performing the averaging or ansatz at the equations of motion level [15–18], but importantly, many methods rely on producing an effective, low-frequency description of the Hamiltonian [19]. The ones most relevant to this work include Lie perturbation theory methods (also known as the "Kamiltonian" method) [14,20,21] and methods based on a systematic perturbation theory leveraging the Schrieffer-Wolff transformation [22] and Floquet theory [23–25], as well as high-frequency expansions [26]. These methods produce an effective static Hamiltonian description that encodes some of the effects of the fast dynamics in a low-frequency description. Other methods describe the time-coarse-grained evolution in terms of a Liouville equation; notable examples include the Keldysh-Lindblad expansion [27] and the TCG method [2,7,28] which can be thought of as a generalization of the effective Hamiltonian methods. The TCG method also captures nonunitary effects that account for the information lost during coarse-graining. This is achieved by one taking a moving average over the expanded generator, rather than the Hamiltonian. Among other things, this allows us to consider off-resonant virtual transitions as well as resonant multibody transitions, such as two-photon processes,

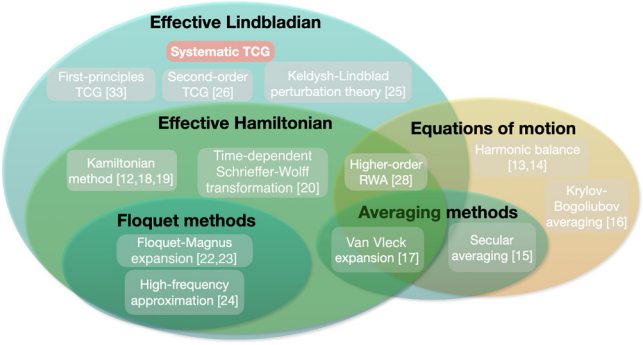

FIG. 3. A Venn diagram of different methods dealing with time-dependent driven systems. The bold black headings indicate the level of operation of the method, and the gray squares indicate different methods. TCG generalizes many current methods to include nonunitary contributions. Systematic TCG (this work, in red) permits the TCG calculation to any order, and for more general regimes.

which are omitted in the (first-order) RWA [29]. In addition, the resulting terms are weighted in a way that is fine-tuned to the chosen measurement resolution and the form of the filter function. STCG differs from effective Hamiltonian approaches in several ways: (1) Even starting with a Hamiltonian of a system with finite degrees of freedom it produces a Liouvillian that captures the nonunitary effects due to time-averaging, as illustrated in Fig. 4, giving a more comprehensive description of the low-frequency dynamics. As we will show with examples, the nonunitary effects can be important in the presence of strong and/or time-varying drives, or certain initial conditions. (2) TCG is generalizable to systems with infinitely many degrees of freedom [30–32], producing an effective non-Markovian dynamics of a subsystem consistent with the coarse-graining timescale desired.

Our method, STCG, provides a systematic framework for generalizing the RWA and other effective Hamiltonian methods into a Lindblad-like generator, and allows TCG to be performed to an arbitrary degree of accuracy when suitable conditions are satisfied. Time-coarse-graining was introduced in Refs. [2,28,33,34], and the time-coarse-grained generator has been explicitly derived up to the second order in the coupling constants, under the assumption that the transition frequencies are either much greater or much smaller than τ^{-1}. Our method, as presented in this work, is fully systematic, supported by a diagrammatic expansion, and is capable of explicitly calculating the effective TCG Liouvillian at any order in the coupling constants, while allowing for the most general coarse-graining timescale τ. Furthermore, our method has additional advantages over standard TCG approaches—STCG is more general than standard TCG methods, allowing for arbitrary filter functions $f_\tau(\omega)$ applied by the measurement device.

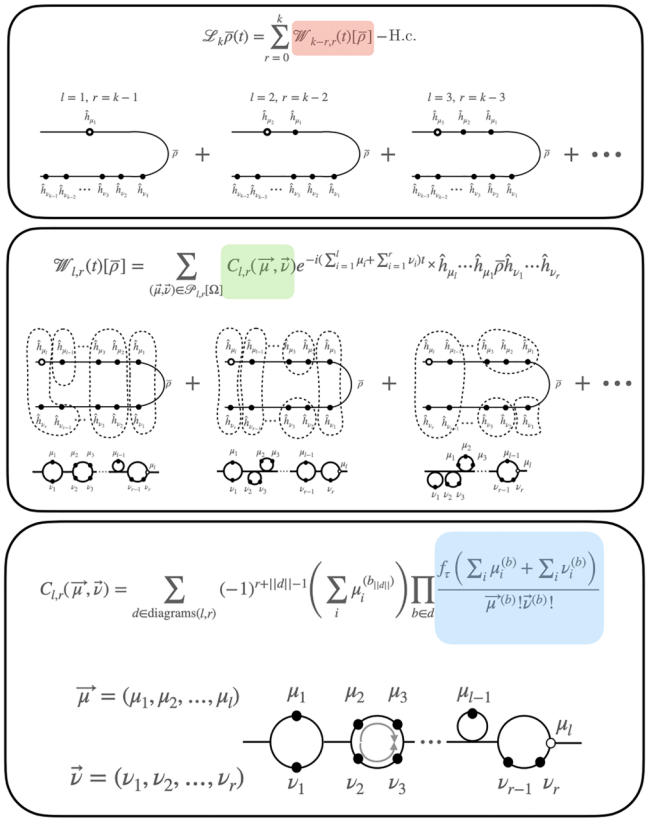

FIG. 4. Top: The TCG Liouvillian can be written as a sum of contraction superoperators $\mathcal{W}_{k-r,r}$, each representing a superoperator with l operators to the left and r operators to the right of $\overline{\rho}$, such that $l + r = k$. Middle: The contribution of each superoperator term is weighted by the contraction coefficients $C_{l,r}$, which encode the contributions from all the different ways one can partition the operators into groups. We represent these partitions with "bubble" diagrams (note that the order is inverted). Bottom: The contribution of each diagram is computed in STCG through a closed-form formula, where each bubble contributes a factor to a product.

IV. SYSTEMATIC TIME-COARSE-GRAINING BY DIAGRAMMATIC EXPANSION

Since the time-coarse-graining procedure inherently erases information, the time evolution of $\overline{\rho}(t)$ cannot be generated by a Hamiltonian in general. We can only assume that the equation of motion for $\overline{\rho}(t)$ is linear and trace-preserving, since these two properties are respected by both the time-coarse-graining process and the underlying von Neumann equation. Consequently, the correct ansatz is a Liouville-like equation that we refer to as the "TCG master equation":

$$i\frac{\partial}{\partial t}\overline{\rho}(t) = \mathcal{L}\overline{\rho}(t). \tag{13}$$

Because the time-coarse-graining operation on $\rho(t)$ does not commute with frame transformations in general (i.e., slow frequencies in one frame may be fast in a different frame), the TCG master equations obtained in different interaction pictures are physically distinct in principle. However, the choice of the interaction picture is partially determined by the measurement channel through which the quantum system is observed. Take a nondegenerate parametric oscillator for example: if one performs a double homodyne measurement with limited time resolution, the measured observables are obtained from the TCG density matrix $\overline{\rho}(t)$ in a static frame where the signal and idler modes are referenced to their respective frequencies; for a single heterodyne measurement using a common local oscillator, the corresponding frame is instead a symmetric frame where both modes are treated on an equal footing.

For the degrees of freedom that commute with the measured observables, one indeed has some remaining freedom in choosing the interaction picture. However, this choice of the reference frame does not affect the measured observables predicted by $\overline{\rho}(t)$, but affects only how fast (or whether) a perturbative expansion of the Liouvillian $\mathcal{L}$ converges as it affects whether the Hamiltonian $\hat{H}$ can be regarded as "small."

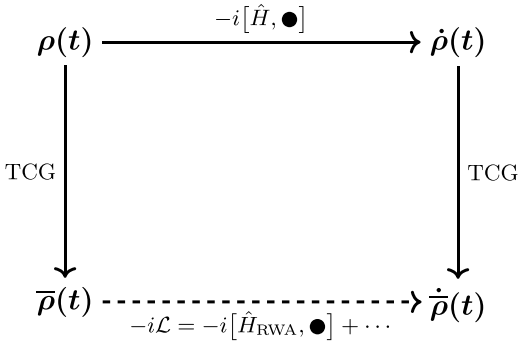

The resulting dynamics of the observables can be shown to be equivalent to the dynamics observed through a band-limited measurement apparatus with a filter function $\tilde{f}_\tau(t)$, with τ parameterizing the coarse-graining timescale. The choice of the interaction picture is thus rendered consequential for the observed physics as it represents the dynamics measured by a given measurement apparatus. We explain this in greater detail in Appendix A in Ref. [7]. In STCG, this determines the frequencies $\omega \in \Omega$ and the associated forms of the different operators $\hat{h}_\omega$ in Eq. (12). These operators appear in conjugate pairs $\hat{h}_\omega = \hat{h}^\dagger_{-\omega}$ due to the hermicity of the Hamiltonian.

In most nontrivial cases, one can obtain only a perturbative formula for $\mathcal{L}$, and for that purpose we assume that this Liouvillian can be expanded as a Dyson series in powers of the interaction-picture Hamiltonian $\hat{H}$:

$$i\frac{\partial}{\partial t}\overline{\rho}(t) = \mathcal{L}\overline{\rho}(t) = \sum_{k=1}^{\infty}\mathcal{L}_k(t)\overline{\rho}(t). \tag{14}$$

Our goal here is to find a closed-form formula for the partial Liouvillian $\mathcal{L}_k$ at each order k, which gives us an effective master equation describing the TCG dynamics as long as the Hamiltonian can be assumed to be "small" for the part of Hilbert space we are interested in. Note that here "small" means that the coupling strengths g_ω are small either in comparison with all energy differences or in comparison with the time-coarse-graining scale τ:

$$g_\omega \ll |\omega - \omega'| \quad \text{for all} \quad \omega,\ \omega', \tag{15a}$$

$$g_\omega \ll 1/\tau \quad \text{for all} \quad \omega. \tag{15b}$$

In particular, we note that the second condition implies that if too much information is coarse-grained away with an exceedingly large τ, important dynamics may be ignored and the perturbative TCG expansion loses its predictive power.

Low-order formulas for $\mathcal{L}_k$ have been obtained by iterative and perturbative solving of the coupled equations of the maps $\rho(0) \to \overline{\rho}(t)$ and $\overline{\rho}(t) \to \rho(0)$ [2,32]. The increasing complexity of the coupled equations prevents efficient calculation of $\mathcal{L}_k$ for $k > 3$, and the resulting expressions for $\mathcal{L}_k$ are seemingly structureless nested averages of the form

$$\mathcal{L}_3\overline{\rho} = \overline{\hat{H}\hat{U}_2\overline{\rho}} - \overline{\hat{H}\overline{\hat{U}_2\overline{\rho}}} - \overline{\hat{H}\overline{\hat{U}_1\overline{\rho}\hat{U}_1^\dagger}} + 2\overline{\hat{H}\overline{\hat{U}_1\overline{\rho}}\hat{U}_1^\dagger} + \cdots, \tag{16}$$

where we use the overline to denote the time average of any function of t defined in the same fashion as in Eq. (1), and $\hat{U}_n(t)$ is defined as the nth-order term in the Dyson series

$$\begin{aligned}\hat{U}_n(t) &= -i\int_0^t dt'\hat{H}(t')\hat{U}_{n-1}(t') \\ &= \sum_{j=0}^{n}(-i)^j\int_0^t\cdots\int_0^{t_{j-1}} dt_1\cdots dt_j \times \hat{H}(t_1)\cdots\hat{H}(t_j).\end{aligned} \tag{17}$$

However, if one explicitly calculates the nested averages in Eq. (16), one would immediately find massive cancellation among the terms, as shown in Supplemental Material [6]. This massive cancellation becomes much more significant at higher orders, which indicates hidden structures in the nested averages that can be used to significantly simplify the algebra.

In this work, we develop the TCG method into a systematic perturbation theory where the structure of $\mathcal{L}_k$ is explored in detail, leading to an explicit closed-form formula for $\mathcal{L}_k$ that can be calculated by computer-algebra systems to arbitrary orders. The first crucial step toward achieving this objective is the following recursive formula for $\mathcal{L}_k$ (the derivation of which can be found in Supplemental Material [6]):

$$\begin{aligned}\mathcal{L}_k(t)\overline{\rho} = &\sum_{l=1}^{k}\left(\overline{\hat{H}\hat{U}_{l-1}\overline{\rho}\hat{U}_{k-l}^\dagger}(t) - \overline{\hat{U}_{l-1}\overline{\rho}\hat{U}_{k-l}^\dagger\hat{H}}(t)\right) \\ &- \sum_{k'=0}^{k-1}\mathcal{L}_{k'}(t)\sum_{l=0}^{k-k'}\overline{\hat{U}_l\overline{\rho}\hat{U}_{k-k'-l}^\dagger},\end{aligned} \tag{18}$$

where we define $\mathcal{L}_0\overline{\rho} \equiv 0$ for any density matrix $\overline{\rho}$. Starting from Eq. (18), one can show that the terms in $\mathcal{L}_k$ can be rearranged into "contraction superoperators" that allow both diagrammatic representation and closed-form formulas. The following subsection is dedicated to the discussion of these contraction superoperators.

A. Diagrammatic expansion and the contraction coefficients

In Ref. [28], the corrections $\overline{\hat{H}\hat{U}_1\overline{\rho}}$ and $-\overline{\hat{H}\hat{U}_1}\overline{\rho}$ in $\mathcal{L}_2\overline{\rho}$ are grouped together and denoted by the contraction $\overline{\hat{H}\hat{U}_1}\,\overline{\rho}$ for convenience. The same is true for two-point contractions of the type $\overline{\hat{H}\overline{\rho}\hat{U}_1^\dagger} \equiv \overline{\hat{H}\overline{\rho}\hat{U}_1^\dagger} - \overline{\hat{H}}\overline{\rho}\overline{\hat{U}_1^\dagger}$. Assuming a Hamiltonian of the form in Eq. (12), we first observe that the cancellation pointed out in the previous section occurs within each such a contraction in $\mathcal{L}_2$. Furthermore, each of the surviving superoperators will have a frequency equal to the sum of the frequencies of the operators involved, which is not true for the individual nested averages constituting the contraction. We show in Supplemental Material [6] that the contractions must be generalized to exhibit this mass cancellation and homogeneous time dependence at all orders. An unexpected byproduct of this finding is that a closed-form expression can be found that is amenable to symbolic computation in a generic manner. Here we summarize the key steps in the derivation, and the interested reader is referred to the Supplemental Material [6].

According to Eq. (18), the nested averages in $\mathcal{L}_k\overline{\rho}$ always have $\hat{H}(t)$ at either the left end or the right end of the product. Therefore, we make the ansatz that the partial Liouvillian $\mathcal{L}_k$ at order $k \geq 1$ can be expressed as a sum over all such generalized contractions with weights (l, r) such that $l + r = k$:

$$\mathcal{L}_k\overline{\rho}(t) = \sum_{r=0}^{k}\mathcal{W}_{k-r,r}(t)[\overline{\rho}] - \text{H.c.}, \tag{19a}$$

where each contraction $\mathcal{W}_{l,r}(t)[\overline{\rho}]$, whose form is to be found, is the sum of all nested averages that have l (r) operators to the left (right) of $\overline{\rho}$, with the leftmost operator being $\hat{H}$. These contractions can always be written as

a sum of operator products with a simple homogeneous harmonic time dependence.

We next write each contraction in the following form:

$$\mathcal{W}_{l,r}(t)[\overline{\rho}] = \sum_{(\vec{\mu},\vec{\nu})\in\mathcal{P}_{l,r}[\Omega]} C_{l,r}(\vec{\mu},\vec{\nu}) \times \hat{h}_{\mu_l}\cdots\hat{h}_{\mu_1}\overline{\rho}\hat{h}_{\nu_1}\cdots\hat{h}_{\nu_r} \times e^{-i\left(\sum_{i=1}^{l}\mu_i+\sum_{i=1}^{r}\nu_i\right)t}, \tag{20}$$

where we split the frequencies into two vectors $\vec{\mu}$ ($\vec{\nu}$) for the frequencies of the modes to the left (right) of the density matrix, while the notation $\mathcal{P}_{l,r}[\Omega]$ denotes the set of all possible pairs of vectors $\vec{\mu}$ and $\vec{\nu}$ whose elements are chosen from the Hamiltonian frequencies. Apart from the combinatorics involved in the summation, calculation of the contraction coefficients $C_{l,r}(\vec{\mu},\vec{\nu})$ is the central element of STCG as each of the resulting coefficients encodes contributions from the many different nested time averages in $\mathcal{L}_k$ to a particular superoperator in the sum [6].

The harmonic expansion in Eq. (20) allows us to derive the main result of the STCG method. Using the harmonic ansatz, we can interpret every diagram as contributing a simple term to the contraction coefficients for each combination of mode frequencies involved. We are able to obtain the following closed-form expression for the contraction coefficient $C_{l,r}(\vec{\mu},\vec{\nu})$:

$$C_{l,r}(\vec{\mu},\vec{\nu}) = \sum_{d\in\text{diagrams}(l,r)} (-1)^{r+\|d\|-1}\left(\sum_i \mu_i^{(b_{\|d\|})}\right) \times \prod_{b\in d}\frac{f_\tau\left(\sum_i \mu_i^{(b)}+\sum_i \nu_i^{(b)}\right)}{\vec{\mu}^{(b)}!\vec{\nu}^{(b)}!}, \tag{21}$$

where $d=(b_1,b_2,\ldots,b_{\|d\|})$ represents a particular diagram d by the ordered set of bubbles in d, with $\|d\|$ being the total bubble number, and the vector factorials $\vec{\mu}^{(b)}!$ and $\vec{\nu}^{(b)}!$ are defined in Eq. (22),

$$\vec{\mu}! \equiv \left(\mu_1,\mu_2,\ldots,\mu_{\|v\|}\right)! = (\mu_1+\cdots+\mu_{\|v\|})\cdots(\mu_1+\mu_2)\times\mu_1. \tag{22}$$

Note that the denominator can vanish for certain frequencies, and the limit must be taken carefully. An explicit formula for the limiting case is given in Supplemental Material [6].

In other words, we sum over the diagrams in the set "diagrams(l,r)", which include all partitions of the frequencies into bubbles $\{b\}$ with frequencies $\vec{\mu}^{(b)}$ and $\vec{\nu}^{(b)}$; for each diagram, we then calculate the product of all the bubble factors, and multiply the result by an extra factor of $\sum_i \mu_i^{(b_{\|d\|})}$ and an overall sign. For a detailed proof of Eq. (21), see Supplemental Material [6]. Note that the contraction coefficients are always real if the frequencies of all the original Hamiltonian terms are real. This property ensures that the corresponding TCG effective Hamiltonian and effective (pseudo)dissipator in Sec. IV B are Hermitian at any order k.

Plugging the expansion of the contraction superoperators [Eq. (20)] into the TCG master equation (19), we can write the Liouvillian in terms of the contraction coefficients:

$$\mathcal{L}_k(t)\overline{\rho} = \sum_{l=1}^{k}\sum_{\vec{\mu},\vec{\nu}\in\mathcal{P}_{l,k-l}[\Omega]}\Big[C_{l,k-l}(\vec{\mu},\vec{\nu})e^{-i(\sum_i\mu_i+\sum_i\nu_i)t} \times \hat{h}_{\mu_l}\cdots\hat{h}_{\mu_1}\rho\hat{h}_{\nu_1}\cdots\hat{h}_{\nu_r} - \text{H.c.}\Big]. \tag{23}$$

Note that, in general, if we have a number of $|\Omega|$ unique frequency-operator pairs in the original Hamiltonian, then for each $l\in\{1,2,\ldots,k\}$, the contraction would be a sum of $|\mathcal{P}_{l,r}[\Omega]| = |\Omega|^{l+r} = |\Omega|^k$ unique terms. To a large extent, this is where the complexity of STCG stems from, and why we complement the analytical formula with a symbolic computational tool.

B. The effective TCG Hamiltonian and pseudodissipators

The structure of the contraction superoperators allows us to separate the different terms in the Liouvillian into Hamiltonian terms and pseudodissipator terms, akin to a Lindblad-type equation. The contraction coefficients satisfy the following symmetries:

$$C_{l,r}(-\vec{\mu},-\vec{\nu}) = (-1)^{l+r-1}C_{l,r}(\vec{\mu},\vec{\nu}), \tag{24a}$$

$$C_{l,r}(\vec{\mu},\vec{\nu}) = C_{r+1,l-1}\left(-(\nu_1,\nu_2,\ldots,\nu_r,\mu_l) - (\mu_1,\mu_2,\ldots,\mu_{l-1})\right). \tag{24b}$$

Using Eq. (24b), we can write the TCG partial Liouvillian at order k as $\mathcal{L}_k = \mathcal{L}_k^H + \mathcal{L}_k^\gamma$, with

$$\mathcal{L}_k^H\overline{\rho} = [\hat{\mathcal{H}}_k,\overline{\rho}], \tag{25a}$$

$$\mathcal{L}_k^\gamma\overline{\rho} \equiv i\hat{D}_{\text{TCG}}^{(k)}\overline{\rho} = \sum_{l=1}^{k-1}\sum_{\vec{\mu},\vec{\nu}\in\mathcal{P}_{l,k-l}[\Omega]} i\gamma_{\vec{\mu},\vec{\nu}}^{(k)}e^{-i\sum_j(\mu_j+\nu_j)t}\mathcal{D}[\hat{L}_{\vec{\mu}},\hat{J}_{\vec{\nu}}]\overline{\rho}, \tag{25b}$$

where $\hat{H}_k$ and $\hat{D}_{\text{TCG}}^{(k)}$ can both be explicitly written in terms of the contraction coefficients $C_{l,r}(\vec{\mu},\vec{\nu})$ in Eq. (21). As usual, this decomposition of $\mathcal{L}_k$ into Hermitian Hamiltonian terms and trace-preserving (pseudo)dissipators is not the only option, and alternative representations also exist. One option is to absorb the anticommutator terms into the Hamiltonian, portraying the dynamics as a (generally non-Hermitian) Hamiltonian with virtual jumps. This

representation can be convenient for specific problems, but it does not alter the underlying physics.

The Hamiltonian terms in Eq. (25) are one-sided, having operators multiplied only to the left or the right of the density matrix. In the rest of this work, we represent $\hat{\mathcal{H}}_k$ as three vectors of equal length, where the nth elements of the vectors represent the coefficient, the operator, and the frequency of the nth contraction term in $\hat{\mathcal{H}}_k$, respectively:

$$q^{(k)}_{\vec{\mu}} = \frac{1}{2}\left(C_{k,0}(\vec{\mu}) + C_{k,0}(-\vec{\mu}^{\,\mathrm{rev}})\right)\prod_{\omega\in\vec{\mu}} g_\omega, \tag{26a}$$

$$\hat{s}^{(k)}_{\vec{\mu}} = \hat{h}_{\mu_k}\hat{h}_{\mu_{k-1}}\cdots\hat{h}_{\mu_1}, \tag{26b}$$

$$\Omega^{(k)}_{\vec{\mu}} = \sum_{\mu_i\in\vec{\mu}} \mu_i, \tag{26c}$$

where $\vec{\mu}\in\mathcal{P}_{k,0}[\Omega]$, $\vec{\mu}^{\,\mathrm{rev}} := (\mu_k, \mu_{k-1}, \ldots, \mu_1)$ denotes the reverse of $\vec{\mu} = (\mu_1, \mu_2, \ldots, \mu_k)$, and $\mathcal{P}_{l,r}[\Omega]$ is defined as the set of two-vector pairs of lengths l and r, where each component is drawn from Ω with repetition. The total effective Hamiltonian to order k can then be written as

$$\begin{aligned}\hat{H}^{(k)}_{\mathrm{TCG}}(t) &= \sum_{k'=1}^{k}\hat{\mathcal{H}}_{k'}(t)\\ &= \sum_{k'=1}^{k}\sum_{\vec{\mu}\in\mathcal{P}_{k',0}[\Omega]} g^{(k')}_{\vec{\mu}} e^{-i\sum_{j=1}^{k'}\mu_j t}\hat{h}_{\mu_{k'}}\hat{h}_{\mu_{k'-1}}\cdots\hat{h}_{\mu_1}.\end{aligned} \tag{27}$$

The (pseudo)dissipator terms, on the other hand, are generalizations of Lindblad dissipators that assume a more general form and can be written as $\mathcal{D}[\hat{L},\hat{J}]$ for some operators $\hat{L}$ and $\hat{J}$ so that it acts on any density matrix ρ as

$$\mathcal{D}[\hat{L},\hat{J}]\rho = \hat{L}\rho\hat{J} - \frac{1}{2}\{\hat{J}\hat{L},\rho\}. \tag{28}$$

Notice that these (pseudo)dissipators become the usual diagonal Lindblad dissipators if $\hat{J} = \hat{L}^\dagger$, but this form is not generally possible. The Hamiltonian terms appear only on one side of the density matrix, while the generalized Lindblad dissipators $\mathcal{D}[\hat{L}_{\vec{\mu}},\hat{J}_{\vec{\nu}}]$ act on both sides of $\overline{\rho}(t)$. Therefore, for each dissipator term, we need to specify a pair of operators $(\hat{L}_{\vec{\mu}},\hat{J}_{\vec{\nu}})$. Using similar notation as before, we can represent the kth-order effective dissipator terms by three vectors of the coefficients, the operator pairs $\{(\hat{L}_{\vec{\mu}},\hat{J}_{\vec{\nu}})\}$, and the corresponding frequencies, respectively:

$$i\gamma^{(k)}_{\vec{\mu},\vec{\nu}} = \left\{\left(C_{l,r}(\vec{\mu},\vec{\nu}) - C_{r,l}(-\vec{\nu}^{\,\mathrm{rev}},-\vec{\mu}^{\,\mathrm{rev}})\right) \times \prod_{\mu_i\in\vec{\mu}} g_{\mu_i}\prod_{\nu_i\in\vec{\nu}} g_{\nu_i} \mid (\vec{\mu},\vec{\nu})\in\mathcal{P}_{l,r}[\Omega]\right\}, \tag{29a}$$

$$\left(\hat{L}_{\vec{\mu}},\hat{J}_{\vec{\nu}}\right) = \left\{\left(\hat{h}_{\mu_l}\hat{h}_{\mu_{l-1}}\cdots\hat{h}_{\mu_1},\hat{h}_{\nu_1}\hat{h}_{\nu_2}\cdots\hat{h}_{\nu_r}\right) \times \mid (\vec{\mu},\vec{\nu})\in\mathcal{P}_{l,r}[\Omega]\right\}, \tag{29b}$$

$$\Omega_{\vec{\mu},\vec{\nu}} = \left\{\sum_{\mu_i\in\vec{\mu}}\mu_i + \sum_{\nu_i\in\vec{\nu}}\nu_i \mid (\vec{\mu},\vec{\nu})\in\mathcal{P}_{l,r}[\Omega]\right\}, \tag{29c}$$

where we range over all positive integers (l,r) such that $l+r=k$.

According to the Gorini-Kossakowski-Sudarshan-Lindblad theorem [35,36], a necessary condition for the evolution of $\overline{\rho}(t)$ to be a completely positive map is that the matrix $[\gamma_{ij}]$ is positive definite. It is important to note that this condition is not satisfied by the TCG effective dissipators in general. This is not a problem as not all Hermitian positive semidefinite density matrices are possible in the coarse-grained world. For example, when the interaction-picture Hamiltonian $\hat{H}$ is time dependent, there is no time-independent pure state ρ that commutes with $\hat{H}$, and consequently the resulting coarse-grained $\overline{\rho}(t)$ cannot be a pure state in general. Indeed, one must keep in mind that $\overline{\rho}(t)$ does not represent the quantum state of the system at any particular moment in time; rather, it is a phenomenological object that allows one to calculate the time-coarse-grained observables. Therefore, even when $[\gamma_{ij}]$ is not positive definite, the corresponding TCG master equation can still describe well-behaved time evolution without generating negative probabilities if the initial state is allowed in the time-coarse-grained picture [37–39].

Summing over all these terms up to order k, we obtain the following total effective (pseudo)dissipator:

$$\hat{D}^{(k)}_{\mathrm{TCG}}[\overline{\rho}](t) \equiv \sum_{l=1}^{k-1}\sum_{(\vec{\mu},\vec{\nu})\in\mathcal{P}_{l,r}[\Omega]} \gamma^{(k)}_{\vec{\mu},\vec{\nu}} \times \mathcal{D}[\hat{L}_{\vec{\mu}},\hat{J}_{\vec{\nu}}]\overline{\rho} \times e^{-i\left(\sum_{j=1}^{l}\mu_j + \sum_{j=1}^{r}\nu_j\right)t}. \tag{30}$$

Note that for $k=1$, we get no effective dissipators since there are no double-sided terms, and the corresponding effective Hamiltonian is simply the time-coarse grained

original Hamiltonian:

$$\hat{H}^{(1)}_{\mathrm{TCG}}(t) = \sum_{\omega} f_\tau(\omega) e^{-i\omega t}\hat{h}_\omega = \int_{-\infty}^{\infty} dt' \tilde{f}_\tau(t-t')\hat{H}(t'). \tag{31}$$

For a physical coarse-graining window function $\tilde{f}_\tau(t)$, the Fourier transform $f_\tau(\omega) \equiv \int_{-\infty}^{\infty} dt \times \tilde{f}_\tau(t) e^{i\omega t}$ can be considered as a low-pass filter in the interaction picture, which manifestly suppresses the coefficients of the high-frequency terms in $\hat{H}(t)$. In the laboratory frame, however, the function $f_\tau(\omega)$ effectively applies a bandpass filter to all the terms in the Hamiltonian. Therefore, our ignoring the small terms in $\hat{H}^{(1)}_{\mathrm{TCG}}(t)$ (rather than the "high-frequency" terms by some ambiguous standard) would give us the RWA Hamiltonian. In this sense, the RWA can be considered as the lowest-order TCG with suitable choices of the coarse-graining timescale to suppress the high-frequency terms.

In higher orders of the theory, one typically begins to see the appearance of effective (pseudo)dissipators. Depending on the quantum system, these (pseudo)dissipators may either account for microfluctuations in the entropy and energy due to time-coarse-graining, or represent secular energetic loss or gain through high-frequency channels or nonadiabatic effects, depending also on whether the rates are real or imaginary. According to our experience, the latter situation usually occurs in systems with resonant drives, parametric time dependence, or external heat reservoirs. These (pseudo)dissipators are an important aspect of the STCG method, since they cannot be properly accounted for by any effective Hamiltonian approaches commonly used in such situations, such as Floquet or Kamiltonian methods. Rather, they represent corrections of a different type, which are usually ignored in effective theories but can prove to be important for modeling the long-time dynamics of certain quantum systems.

V. EXAMPLES

To showcase the capabilities and use cases of STCG, we demonstrate it on two select examples. The driven Kerr parametron, where we show how it can be used to analyze adiabatic and nonadiabatic effects, and the driven Duffing oscillator, where we show that STCG produces all the terms produced by the Kamiltonian methods, while complementing them with additional nonunitary corrections.

A. Driven Kerr parametron

The Kerr parametron is a phase-locked parametric oscillator, which bifurcates between two possible opposite phases when driven by an oscillating pump field at approximately twice their natural frequency. In the quantum regime, the parametron can exist in a superposition of these two phase states, known as a cat state, acting as an effective biased-error qubit [40]. The cat state generated is fragile, and the parametron decay causes it to quickly decohere, necessitating rapid controls. These rapid controls must adhere to two conflicting requirements. On the one hand, they require a large pump field to prevent unwanted nonadiabatic transitions. On the other hand, large pump fields degrade qubit coherence by introducing unwanted nonresonant rapidly oscillating terms (NROTs). This is a prime use case for the time-coarse-graining method, which allows us to generally consider the contribution of these NROTs. This trade-off and optimization was studied by Masuda *et al.* [4], and we show here that our method reproduces their numerical results and generalizes their effective model to capture unitary and nonunitary corrections.

The parametron is composed of a superconducting quantum interference device array resonator with N superconducting quantum interference devices, which can be represented in the interaction picture in the rotating frame at $\omega_p/2$ by an effective Hamiltonian,

$$\hat{H} = (\Delta + \chi)\,\hat{a}^\dagger\hat{a} - \frac{\chi}{12}\left(\hat{a}e^{-i(\omega_p/2)t} + \hat{a}^\dagger e^{+i(\omega_p/2)t}\right)^4 + 2\beta(\hat{a}e^{-i(\omega_p/2)t} + \hat{a}^\dagger e^{i(\omega_p/2)t})^2\cos\left(\omega_p t\right), \tag{32}$$

where $\Delta \equiv \omega_c^{(0)} - \chi - \omega_p/2$ is the detuning from the "bare" resonance frequency $\omega_c^{(0)} = \sqrt{8E_C E_J/N}$. In addition, $\chi = E_C/N^2$ is the nonlinear coefficient strength and $\beta = \omega_c^{(0)}(\delta E_J/8E_J)$ is the pump strength. This form of the Hamiltonian is correct in the regime $\chi\beta \ll (\omega_c^{(0)})^2$. As explained in Ref. [4], both the pump strength β and the detuning Δ can be made time dependent by one simultaneously tuning ω_c^0 and δE_J. In particular, Masuda *et al.* [4] consider a particular driving schedule for β and Δ for $0 \le t \le T$:

$$\beta(t) = \beta_0\frac{t}{T}, \quad \Delta(t) = \Delta_0\left(1 - \frac{t}{T}\right). \tag{33}$$

Although it is shown that the fidelity of the process depends significantly on the non-RWA terms in the Hamiltonian (also referred to as the "NROTs"), there is no analytical formula that quantifies their long-term effects over a timescale much greater than ω_p^{-1}. Moreover, in addition to the non-RWA terms, nonadiabatic effects also play a significant role in the performance of the device, and are considered in the literature to be completely independent of the non-RWA effects. Here we perform the analysis using STCG, and show how both effects can be captured by it, and that the two are not entirely separate phenomena. Following Masuda *et al.* [4], we assume the following numerical values of the parameters:

$$\begin{aligned} \omega_p/2\pi &= 16\,\mathrm{GHz}, \quad \Delta_0/2\pi = -67\,\mathrm{MHz}, \\ \beta_0/2\pi &= 200\,\mathrm{MHz}, \quad \chi/2\pi = 68\,\mathrm{MHz}, \end{aligned} \tag{34}$$

with $T = 50$ ns. Although the linear time dependence in the coefficients Δ and β may appear incompatible with STCG, which assumes that the Hamiltonian can be written as a discrete Fourier series as in Eq. (12), time dependent terms of the form $gte^{i\omega t}$ can nevertheless arise in the limit:

$$gte^{i\omega t} = \lim_{\delta\to 0} \frac{ge^{i(\omega+\delta)t} - ge^{i\omega t}}{i\delta}. \tag{35}$$

Using that expansion, we can represent $\hat{H}$ by the following three lists of coefficients, rotating-frame frequencies, and Hamiltonian operators:

$$\begin{aligned} g_\Omega = \Big\{ &\frac{\beta_0}{i\delta T}, -\frac{\beta_0}{i\delta T}, \frac{\beta_0}{i\delta T}, -\frac{\beta_0}{i\delta T}, -\frac{\beta_0}{i\delta T}, \frac{\beta_0}{i\delta T}, -\frac{\beta_0}{i\delta T}, \\ &\frac{\beta_0}{i\delta T}, -\frac{2\beta_0}{i\delta T}, \frac{2\beta_0}{i\delta T}, \frac{2\beta_0}{i\delta T}, -\frac{2\beta_0}{i\delta T}, \Delta_0, -\frac{\Delta_0}{2i\delta T}, \frac{\Delta_0}{2i\delta T}, \\ &-\frac{\chi}{2}, -\frac{\chi}{2}, -\frac{\chi}{3}, -\frac{\chi}{2}, -\frac{\chi}{3}, -\frac{\chi}{12}, -\frac{\chi}{12} \Big\}, \end{aligned} \tag{36a}$$

$$\begin{aligned} \Omega = \big\{ &\delta, 0, 2\omega_p + \delta, 2\omega_p, -\delta, 0, -2\omega_p - \delta, \\ &-2\omega_p, -\omega_p - \delta, -\omega_p, \omega_p + \delta, \omega_p, 0, \delta, \\ &-\delta, 0, -\omega_p, -\omega_p, \omega_p, \omega_p, -2\omega_p, 2\omega_p \big\}, \end{aligned} \tag{36b}$$

$$\begin{aligned} h_\Omega = \big\{ &\hat{a}^{\dagger 2}, \hat{a}^{\dagger 2}, \hat{a}^{\dagger 2}, \hat{a}^{\dagger 2}, \hat{a}^2, \hat{a}^2, \hat{a}^2, \hat{a}^2, \hat{a}^\dagger\hat{a}, \hat{a}^\dagger\hat{a}, \hat{a}^\dagger\hat{a}, \hat{a}^\dagger\hat{a}, \\ &\hat{a}^\dagger\hat{a}, \hat{a}^\dagger\hat{a}, \hat{a}^\dagger\hat{a}, \hat{a}^{\dagger 2}\hat{a}^2, \hat{a}^2, \hat{a}^\dagger\hat{a}^3, \hat{a}^{\dagger 2}, \hat{a}^{\dagger 3}\hat{a}, \hat{a}^4, \hat{a}^{\dagger 4} \big\}. \end{aligned} \tag{36c}$$

The number of TCG contributions is huge; however, the highly oscillatory terms at frequencies of order ω_p are exponentially suppressed, and can therefore be ignored in the TCG master equation. The long-term effects of the high-frequency transitions are captured by slow-varying corrections to the RWA Hamiltonian as well as emergent high-order pseudodissipators. Therefore, we set a threshold and keep only the TCG contribution with coefficients greater than 0.08 MHz for a coarse-graining timescale τ of 0.125 ns. The TCG effective Hamiltonian and dissipators can be written as

$$\begin{aligned} \hat{H}_{\mathrm{TCG}}(t) = &g_{11}\hat{a}^\dagger\hat{a} + g_{22}\hat{a}^{\dagger 2}\hat{a}^2 + g_{33}\hat{a}^{\dagger 3}\hat{a}^3 \\ &+ \left(g_{20}\hat{a}^{\dagger 2} + g_{31}\hat{a}^{\dagger 3}\hat{a} + \mathrm{H.c.}\right), \end{aligned} \tag{37}$$

$$\begin{aligned} \hat{D}_{\mathrm{TCG}}(t) = &\Gamma_{2,0;0,2}\mathcal{D}[\hat{a}^{\dagger 2}, \hat{a}^2] + \Gamma_{0,2;2,0}\mathcal{D}[\hat{a}^2, \hat{a}^{\dagger 2}] \\ &+ \big(\Gamma_{2,0;2,0}\mathcal{D}[\hat{a}^{\dagger 2}, \hat{a}^{\dagger 2}] + \Gamma_{2,0;2,2}\mathcal{D}[\hat{a}^{\dagger 2}, \hat{a}^{\dagger 2}\hat{a}^2] \\ &+ \Gamma_{0,2;2,2}\mathcal{D}[\hat{a}^2, \hat{a}^{\dagger 2}\hat{a}^2] + \Gamma_{1,1;2,0}\mathcal{D}[\hat{a}^\dagger\hat{a}, \hat{a}^{\dagger 2}] \\ &+ \Gamma_{1,1;0,2}\mathcal{D}[\hat{a}^\dagger\hat{a}, \hat{a}^2] + \mathrm{H.c.}\big), \end{aligned} \tag{38}$$

respectively, with the notation $\mathcal{D}[\cdot,\cdot]$ used as defined in Eq. (28). The analytical expressions for the (super)operator coefficients are given in Supplemental Material [6]. As a baseline, we note that after truncation of terms exponentially suppressed by factors of $e^{-(\omega_p^2\tau^2/2)}$, the first-order TCG master equation is identical to the von Neumann equation under the RWA. The corresponding RWA Hamiltonian can then be written as

$$\hat{H}_{\mathrm{RWA}}(t) = g_{11}^{\mathrm{RWA}}\hat{a}^\dagger\hat{a} + g_{22}^{\mathrm{RWA}}\hat{a}^{\dagger 2}\hat{a}^2 + \left(g_{20}^{\mathrm{RWA}}\hat{a}^{\dagger 2} + \mathrm{H.c.}\right), \tag{39}$$

with the following effective couplings:

$$g_{11}^{\mathrm{RWA}} = \Delta(t), \quad g_{22}^{\mathrm{RWA}} = -\frac{\chi}{2}, \quad g_{20}^{\mathrm{RWA}} = \beta(t). \tag{40}$$

The additional corrections in Eqs. (37) and (38) come from the higher-order TCG perturbative expansion. Let us focus our discussion on three representative Hamiltonian coefficients for the renormalized detuning. We focus on these three because they represent three important cases: g_{11}—a Hamiltonian term with nonadiabatic and non-RWA contributions; $\Gamma_{2,0;0,2}$—a fully nonadiabatic dissipator; and $\Gamma_{1,1;2,0}$—a pseudodissipator with both non-RWA and nonadiabatic contributions. From the analytical expressions for the corrections, one sees that the non-RWA effects and the nonadiabatic effects are not completely separable. By considering the dependencies on T and ω_p, we can identify which contributions come from nonadiabatic effects and which come from non-RWA effects. Here, we present the corrections to the effective couplings in Eq. (40), as obtained from STCG:

$$\begin{aligned} g_{11} = &\Delta(t) - \frac{2\left(\beta(t)^2 + \beta(\tau)^2\right)}{\omega_p} - \frac{4\chi^2}{\omega_p} \\ &+ \Delta_0\beta(\tau)^2\left(20\tau^2 + \frac{11}{2\omega_p^2}\right) - \Delta(t)\beta(\tau)^2\left(26\tau^2 + \frac{13}{\omega_p^2}\right) \\ &- \left(\frac{\tau^2\Delta_0}{T}\right)^2\Delta(t) + \frac{3}{2}\frac{\beta_0\Delta_0}{T^2\omega_p^4}\beta(t) \\ &+ 2\left(\frac{\beta(t)}{\omega_p}\right)^2\Delta(t) - \frac{51}{2}\left(\frac{\beta_0}{T\omega_p^2}\right)^2\chi \\ &- \left(6\left(\frac{\beta(t)}{\omega_p}\right)^2 - 4\left(\frac{\beta(\tau)}{\omega_p}\right)^2\right)\chi \\ &+ 8\left(\frac{\chi}{\omega_p}\right)^2\Delta(t) - \frac{151\chi^3}{6\omega_p^2}. \end{aligned} \tag{41}$$

Let us consider g_{11} as an example: The correction $-(2\beta(t)^2/\omega_p)$ in g_{11} is purely a non-RWA effect as it comes from the high-frequency Hamiltonian terms $\beta(t)\hat{a}^{\dagger 2}e^{2i\omega_p t}$ and $\beta(t)\hat{a}^2e^{-2i\omega_p t}$, and does not vanish in the adiabatic limit $T \to \infty$. However, the correction

$20\Delta_0\beta(\tau)^2\tau^2$ is purely a nonadiabatic effect as it involves no high-frequency Hamiltonian terms and vanishes as $\beta^2(\tau) \propto T^{-2}$ in the adiabatic limit. The correction $-(2\beta(\tau)^2/\omega_p)$, however, is a joint effect of the non-RWA and nonadiabatic terms in the Hamiltonian since it is produced by the contraction of the high-frequency terms $\beta(t)\hat{a}^{\dagger 2}e^{2i\omega_p t}$ and $\beta(t)\hat{a}^2e^{-2i\omega_p t}$ but vanishes as T^{-2} in the adiabatic limit. The dissipator terms are particularly interesting, since they are unique to the TCG approach. We focus on a select set of dissipative contributions that reveal unique effects captured by the STCG approach. We begin with a purely dissipative contribution:

$$\Gamma_{2,0;0,2} = \frac{\beta_0}{T}\left(2\tau^2 + \frac{1}{2\omega_p^2}\right)\beta(t). \tag{42}$$

Interestingly, $\Gamma_{2,0;0,2}\mathcal{D}[\hat{a}^{\dagger 2}, \hat{a}^2]$ is a fully nonadiabatic effect that receives corrections from the counterrotating terms in the Hamiltonian. Importantly, it has the standard Lindblad form together with a positive transition rate. Therefore, it represents effective dissipative phenomena in the form of two-photon absorption that cannot be analyzed efficiently with only effective Hamiltonian approaches. The non-Hamiltonian contributions arising from STCG do not necessarily follow the standard dissipative forms typically encountered in open quantum systems. They are often non-standard and complex, as illustrated by the following example:

$$\begin{aligned}
\Gamma_{1,1;2,0} = &-\frac{45\beta_0}{2T\omega_p^3}\left(\beta(t)^2 + \beta(\tau)^2\right) \\
&- \frac{2\tau^2\beta_0}{T\omega_p}\left(3\beta(t)^2 + 2\beta(\tau)^2\right) \\
&- \frac{5}{2}\left(2\beta(t) - \beta_0\right)\frac{\tau^2\Delta_0\chi}{T\omega_p} \\
&- \frac{2\Delta_0\chi}{T\omega_p^3}\beta(t) - \frac{19\beta_0\chi^2}{3T\omega_p^3} - \frac{4\tau\chi^2}{\omega_p}\beta(\tau) \\
&+ i\left[3\tau^2\left(\left(\frac{\tau\Delta_0}{T}\right)^2 - 4\beta(\tau)^2\right)\beta(t)\right. \\
&- 4\left(\frac{\tau^2\Delta_0}{T}\right)^2\beta_0 \\
&+ 2\tau\beta(\tau)\left(\frac{\tau^2\Delta_0}{T}\right)\chi + \frac{183}{4}\left(\frac{\beta_0}{T\omega_p^2}\right)^2\beta(t) \\
&- 17\frac{\beta(t)^3}{\omega_p^2} - 39\left(\frac{\beta(\tau)}{\omega_p}\right)^2\beta(t) - \frac{2\beta(t)\Delta(t)}{\omega_p^2}\chi \\
&\left. + \frac{13\tau^2\beta_0\Delta_0\chi}{4T^2\omega_p^2} - \left(\frac{\chi}{\omega_p}\right)^2\beta(t)\right].
\end{aligned} \tag{43}$$

The effective dissipator $\Gamma_{1,1;2,0}\mathcal{D}[\hat{a}^\dagger\hat{a}, \hat{a}^{\dagger 2}]$, on the other hand, does not assume the standard Lindblad form, and has both real and imaginary parts in general. The real part of $\Gamma_{1,1;2,0}$ originates from nonadiabatic effects and vanishes in the $T \to \infty$ limit, whereas the imaginary part of $\Gamma_{1,1;2,0}$ contains purely non-RWA contributions as well—the third-order terms $-17i(\beta(t)^3/\omega_p^2)$, $-i(\chi/\omega_p)^2\beta(t)$, and $-i(2\beta(t)\Delta(t)/\omega_p^2)\chi$ survive the $T \to \infty$ limit. These generalized (pseudo)dissipators are important in the strongly driven regime, but most of them vanish when $\beta_0 \to 0$, leaving only some remnants from the time dependence of $\Delta(t)$.

We emphasize that the symbolic calculation of these coefficients is highly involved, even with the closed-form formula in Eq. (21). It is therefore important that the computation is done fully automatically by a computer-algebra system such as QuantumGraining.jl, in a process that is completely generic and applicable to a very wide range of problems.

An important benefit of the TCG effective master equation is that it allows efficient numerical simulation of the system dynamics, since the effects of virtual transitions to and from the high-energy states are captured by the effective Hamiltonian corrections and emergent dissipators, without requiring detailed knowledge of the dynamics of the those high-energy states and their coherences. As a result, accurate numerical simulation can be done at much lower time resolutions (on the order of τ rather than ω_p^{-1}), and truncation of the Hilbert space in the TCG framework is, in general, more forgiving.

Assuming the parameter values in Eq. (34) and taking the coarse-graining timescale τ to be 0.125 ns, we can truncate the Hilbert space at the 20th level and numerically solve the TCG master equation at different orders. Note that truncation at much higher levels will not increase the accuracy since the quartic expansion of the cosine potential starts to break down above the 20th level for the given parameters. The coarse-grained exact dynamics, on the other hand, is obtained by application of the Gaussian window function on the numerical solution to the von Neumann equation with the original Hamiltonian $\hat{H}(t)$. We emphasize that, compared with the TCG master equations, much smaller time steps have to be taken to overcome the stiffness of the exact equation of motion due to the fast-oscillating nonlinear terms in $\hat{H}(t)$. In addition, solutions to the TCG master equations are more accurate than the RWA solution when benchmarked against the coarse-grained exact dynamics, with the accuracy increasing with the order of the TCG perturbation theory.

We plot the coarse-grained instantaneous ground state population p_0 as a function of time in Fig. 5. In particular, we notice that contrary to the RWA result, higher-order TCG predicts an approximately linear decay in $p_0(t)$ during the later half of the time evolution. For the relatively short

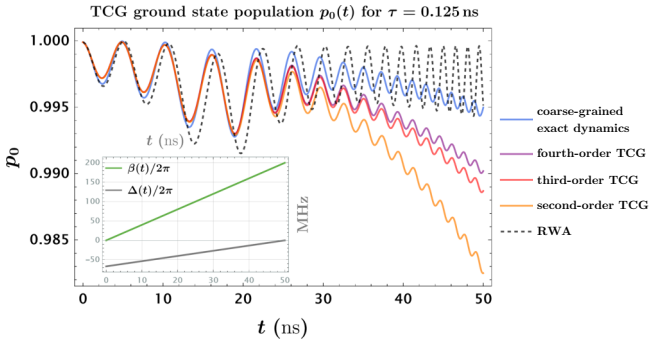

FIG. 5. Instantaneous ground state population p_0 as a function of time, with the use of $\overline{\rho}$ at different orders in TCG. $p_0(50\,\text{ns})$ is defined as the fidelity of the cat-state generation process. The exact ρ is assumed to be in the pure ground state at time $t = -1$ ns, and the initial condition for $\overline{\rho}(t)$ at $t = 0$ is obtained by our time-averaging the numerical solution to the non-TCG von Neumann equation from $t = -1$ ns to $t = 1$ ns.

ramping time T and large initial detuning $|\Delta_0|$, this linear decay is the dominant source of the loss of cat-state fidelity. This has been observed in existing high-time-resolution simulations of the cat-state fidelity (e.g., in Fig. 2 in Ref. [4]), although to our knowledge no explanation for the different behaviors of p_0 during the earlier half and the later half of the time evolution has been provided in the literature.

Using our analytical TCG results, using leading-order perturbation theory for the estimation of $\partial_t|0(t)\rangle$, we obtain the following approximate expression for $\dot{p}_0(t)$:

$$\begin{aligned}\dot{p}_0(t) &\equiv \gamma_{\text{inert}}(t) + \gamma_{\text{dynam}}(t)\\ &= \text{Tr}\left[\partial_t\left(|0(t)\rangle\langle 0(t)|\right)\overline{\rho}(t)\right] + \text{Tr}\left[|0(t)\rangle\langle 0(t)|\partial_t\overline{\rho}(t)\right]\\ &\approx \sum_{n\geq 1}\left(\frac{\langle n(t)|\dot{H}_{\text{TCG}}(t)|0(t)\rangle}{E_0(t) - E_n(t)}\langle 0(t)|\overline{\rho}(t)|n(t)\rangle + \text{c.c.}\right)\\ &\quad + \langle 0(t)|\hat{D}_{\text{TCG}}(t)\overline{\rho}(t)|0(t)\rangle, \end{aligned} \tag{44}$$

where $E_n(t)$ is the energy of the nth instantaneous Hamiltonian eigenstate $|n(t)\rangle$ for $\hat{H}_{\text{TCG}}(t)$, and we have used the immediate corollary that $\langle 0(t)|[-i\hat{H}_{\text{TCG}}(t), \overline{\rho}(t)]|0(t)\rangle = 0$. We observe that the change in p_0 during the earlier half of the time evolution is dominated by the time evolution of the instantaneous ground state $|0(t)\rangle$ [with its contribution to $\dot{p}_0(t)$ defined as the inertial rate of change $\gamma_{\text{inert}}(t)$]. During the later half of the time evolution, the change in p_0 is dominated by the emergent TCG dissipators [with the corresponding contribution to $\dot{p}_0(t)$ defined as the dynamical rate of change $\gamma_{\text{dynam}}(t)$], as shown in Fig. 6. We provide below the expressions for the two contributions to the rate of change of the ground-state population:

$$\begin{aligned}&\gamma_{\text{inert}}(t)\\ &\quad\approx \sum_{n\geq 1}\left(\frac{\langle n(t)|\dot{H}_{\text{TCG}}(t)|0(t)\rangle}{E_0(t) - E_n(t)}\langle 0(t)|\overline{\rho}(t)|n(t)\rangle + \text{c.c.}\right),\\ &\gamma_{\text{dynam}}(t) = \langle 0(t)|\hat{D}_{\text{TCG}}(t)\overline{\rho}(t)|0(t)\rangle. \end{aligned} \tag{45}$$

In particular, we see in Fig. 6 that the inertial rate γ_{inert} is approximately symmetrical around the zero axis, and is responsible for the initial slow oscillations in $p_0(t)$. It dominates over γ_{dynam} at early times, but decays toward zero as the pumping power increases into the strong-drive regime. The dynamical rate γ_{dyanm} ,on the other hand, is induced by the emergent TCG dissipator. We notice that γ_{dyanm} is almost always negative, with its magnitude increasing at early times and oscillating with increasing frequency around a certain negative mean value at late times. Since the mean value of γ_{dyanm} is negative and comparable with the magnitude of the oscillating γ_{inert}, its secular effects dominate over the effect of γ_{inert} at late times. From either the analytical formula for $\hat{D}_{\text{TCG}}(t)$ or numerical simulations, one can predict that increasing the nonlinearity χ will significantly increase the secular effects of γ_{dyanm} while suppressing the transient oscillations due to γ_{inert}; having more rapid state preparation by decreasing T, on the other hand, will increase both γ_{dyanm} and γ_{inert}.

B. The driven Duffing oscillator

The Duffing oscillator is a damped oscillator driven by a nonlinear force, cubic in the displacement of the particle. Despite its simple description, it shows rich phenomena, such as bistability, chaos, and hysteresis. The quantum Duffing oscillator similarly can show a variety of rich quantum phenomena, such as tunneling, squeezing, and entanglement. It has been studied extensively in recent years as a model for a variety of physical systems, including superconducting circuits, trapped ions, and optical cavities, and it is also a popular model system for studying the effects of quantum mechanics on nonlinear systems. Importantly, it has been studied in the supplemental material for a paper by Venkatraman *et al.* [14], showcasing the capabilities of an effective static Hamiltonian method, based on a Lie algebraic approach known as the "Kamiltonian approach." We use that same example to demonstrate here that the STCG algorithm is not only able to reproduce the effective static Hamiltonian in Ref. [14] as the effective TCG Hamiltonian but is also capable of calculating the non-Hamiltonian corrections resulting from time-coarse-graining.

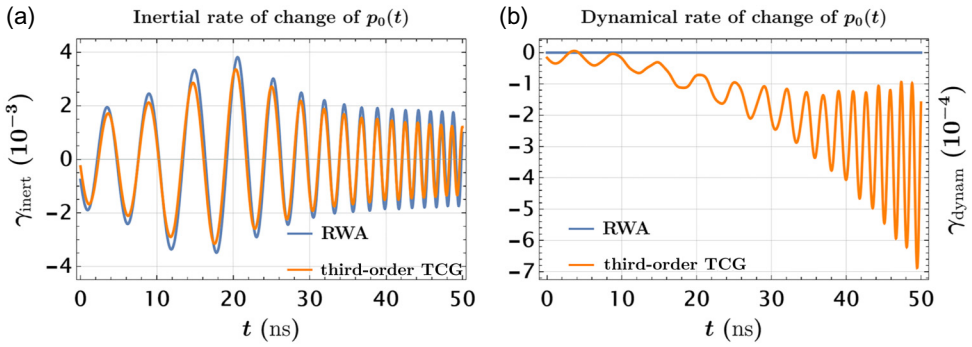

FIG. 6. Time dependence of the inertial and dynamical rates of change for the instantaneous ground state population $p_0(t)$.

The quantum Duffing oscillator is described by the following Hamiltonian:

$$\hat{H} = \delta\hat{a}^\dagger\hat{a} + g_4\left(e^{-i(5/6)\omega_d t}\hat{a} + e^{i(5/6)\omega_d t}\hat{a}^\dagger + e^{-i\omega_d t}\Pi + e^{i\omega_d t}\Pi^*\right)^4. \tag{46}$$

For comparison with the results in Ref. [14], we define $\omega_d \equiv 6\omega$ and round numerical coefficients to the nearest integers. Assuming that $1/g_4, 1/\delta \gg \tau \gg 1/\omega$ and ignoring terms exponentially suppressed by factors of $e^{-(\omega^2\tau^2/2)}$, we can write the fourth-order effective TCG Hamiltonian as

$$\hat{H}^{(4)}_{\text{TCG}}(t) \equiv K^{(4)}_1\hat{a}^\dagger\hat{a} + K^{(4)}_2\hat{a}^{\dagger 2}\hat{a}^2 + K^{(4)}_3\hat{a}^{\dagger 3}\hat{a}^3 + K^{(4)}_4\hat{a}^{\dagger 4}\hat{a}^4 + K^{(4)}_5\hat{a}^{\dagger 5}\hat{a}^5, \tag{47}$$

the coefficients, rounded to the nearest integers, along with the exact analytical formulas, can be found in Supplemental Material [6].

Similarly to the models discussed previously, the TCG effective Hamiltonian (as well as the pseudodissipators) is dependent on the coarse-graining timescale τ in general, and what we present here should be understood as the "IR"-limit results, where τ is much greater than $1/\omega$. In particular, we are able to reproduce all the classical and quantum corrections in the effective Hamiltonian derived in the supplemental material in Ref. [14], demonstrating that the STCG method generalizes the Kamiltonian method, yielding the same time-averaged Hamiltonian for a simple filter function with sufficiently large τ. The agreement between the high-order Hamiltonian corrections obtained by the two distinct methods leads us to conjecture that the effective Kamiltonian can, in general, be obtained by one taking the IR limit of the TCG effective Hamiltonian.

Unlike the parametron control model discussed in the previous subsection, here the coefficients are purely imaginary and, in general, do not have a significant impact on the system dynamics, since the drive on the Duffing oscillator is not resonant with any internal transitions, and there is no parametric time dependence of any sort. In this case, the TCG pseudodissipators provide only quantitative corrections in their range of validity (i.e., when the condition $1/g_4, 1/\delta \gg \tau \gg 1/\omega$ is satisfied). In the following, we numerically simulate the coarse-grained exact dynamics and compare the results with those obtained using TCG and the RWA. The simulations use the following parameter

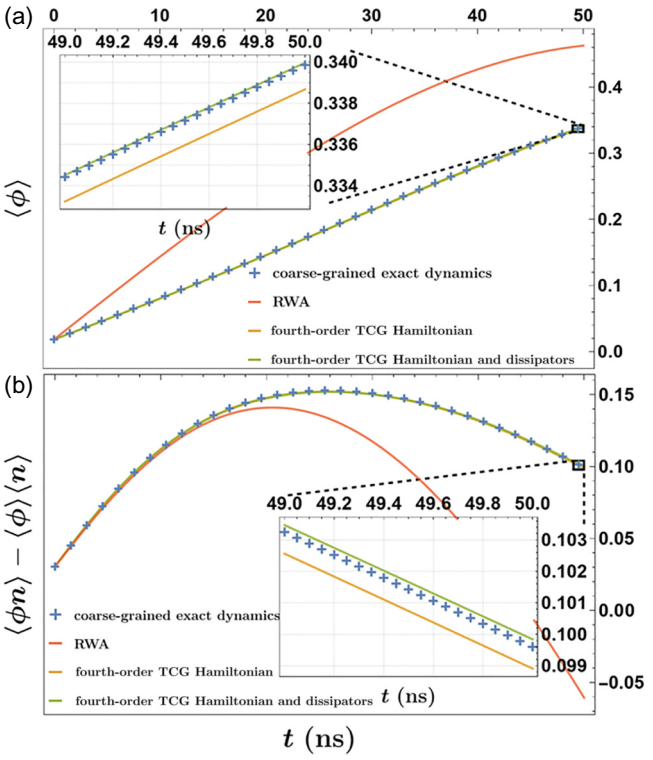

FIG. 7. Time evolution of the (a) quadrature variable $\langle\phi\rangle$ and (b) the correlation $\langle\phi n\rangle - \langle\phi\rangle\langle n\rangle$ simulated with the lowest 25 levels and an initial microscopic (as opposed to coarse-grained) pure coherent state with displacement $\alpha = -0.48i$ at time $t = -3$ ns. The insets show the late-time dynamics in order to show the subtle differences between the different approximations.

values:

$$g_4/2\pi = 0.5\,\mathrm{MHz}, \quad \delta/2\pi = -58.4\,\mathrm{MHz},$$
$$\omega_d/2\pi = 12\,\mathrm{GHz},$$

with driving amplitude $\Pi = 2i$ and time-coarse-graining scale $\tau = 0.5\,\mathrm{ns}$. The numerical simulation of the microscopic von Neumann equation and the TCG master equation (Fig. 7) gives us the following dynamics of the quadrature variable $\langle\phi\rangle$ and the second-order correlation $\langle\phi n\rangle - \langle\phi\rangle\langle n\rangle$, where $\phi \equiv (a + a^\dagger)/\sqrt{2}$ and $n \equiv (a - a^\dagger)/\sqrt{2}i$: Compared directly with coarse-grained dynamics with infinite time resolution, the fourth-order TCG quantum master equation gives much better predictions than the RWA method. However, differently from the parametron example, where the TCG effective dissipators significantly modify the late-time fidelity, here the dynamics is mostly generated by the effective Hamiltonian, with the (pseudo)dissipators giving only minor improvements during later periods of the time evolution. This kind of situation where the effective dynamics is dominated by its coherent part generated by some effective Hamiltonian usually occurs when the external drives have amplitudes that are time independent and frequencies that do not resonate with any internal (virtual) transition processes until very high order in the nonlinearities.

VI. CONCLUSIONS AND OUTLOOK

In the laboratory, the observable dynamics is always time-coarse-grained, due to the finite time resolution of the measurement apparatus. To effectively model these observable dynamics, we introduced the STCG framework, a perturbative series expansion that directly describes the time-coarse-grained observable dynamics of a quantum system. STCG generalizes existing TCG methods to any order, and extends beyond the description given by static effective Hamiltonian approaches [5,14,41] by including nonunitary contributions to the dynamics, which we have shown to be crucial for a correct effective model of the system.

STCG allows a more accurate description of quantum systems in non-RWA regimes and when effective Hamiltonian methods become inadequate, e.g., under strong and fast parametric drives. It gives a description of the time-coarse-grained dynamics in the form of multibody Hamiltonian corrections and (pseudo)dissipators, providing us with an analytical method to identify and study the important emergent processes in regimes where the counterrotating and parametric time-dependent terms become significant. In addition, the diagrammatic representation developed in this work can also help with the design and engineering of the nonlinearities and parametric drives in order to achieve certain effective long-time dynamics. Importantly, the time-coarse-grained description is not only important for analytical studies but is also crucial for numerical analyses, since deep non-RWA regimes are not numerically stable. If the counterrotating terms are included, the equations of motion can require very high time resolutions, with strict constraints on the truncation of the Hilbert space, which can make solving them computationally prohibitive. In addition, these equations can become very stiff and unstable due to the involvement of vastly different timescales and numerous modes. The STCG description, on the other hand, effectively filters the dynamics around a certain frequency band, and accounts for the effects of high-frequency (virtual) transitions in the Hilbert space without needing to keep track of their intricate time evolution. This allows a very efficient numerical study of driven nonlinear quantum systems deep into the non-RWA regime or even when more sophisticated effective Hamiltonian methods fail.

To showcase the STCG method, we used it to study a few problems—the Rabi model, the quantum parametron, and the quantum Duffing oscillator. We have shown that STCG generalizes the existing treatments of these problems, reproducing well-known corrections while revealing nonunitary contributions that are not captured by other methods. Moreover, we have shown that our results match the exact time-coarse-graining of the non-RWA solutions, with the agreement improving for higher orders of approximation. Specifically, we have used the examples to showcase important properties of the STCG method. Using the quantum parametron example, we demonstrated the importance of the nonunitary contributions captured by STCG, which prove to be crucial for correct modeling of the system fidelity and for capturing nonadiabatic effects. Using the quantum Duffing oscillator, we showed that the effective Hamiltonian produced by STCG completely reproduces the effective static Hamiltonian generated by perturbative Lie series approaches, which suggests that effective Hamiltonian approaches may be considered as certain limits of the STCG approach.

The STCG calculation is complex and involved, since it requires the calculation and bookkeeping of many different superoperators that can easily be in the hundreds for a third-order expansion. To aid this situation, we envision the STCG framework as part of a computational framework where the repetitive, intricate procedure is done automatically by a symbolic computation package, aiding the numerical and analytical study of the system. STCG is accompanied by the JULIA software package QuantumGraining.jl [42], which automatically calculates the emergent terms, their coupling strengths, or pseudodissipation rates to help automate analytical and numerical calculations. We hope that the utility and generality of STCG, in addition to the low bar for entry by use of symbolic computation (e.g., with use of QuantumGraining.jl), can make it a valuable tool for theorists and experimentalists alike.

ACKNOWLEDGMENTS

The authors thank Emanuele Dalla Torre for his comments on the manuscript. This work was supported by the U.S. Department of Energy, Office of Basic Energy Sciences, Division of Materials Sciences and Engineering, under Award No. DESC0016011. Support was also provided by the Army Research Office under Contract No. W911NF-23-1-0252.

DATA AVAILABILITY

The data that support the findings of this article are openly available [42].

[1] M. P. Da Silva, D. Bozyigit, A. Wallraff, and A. Blais, Schemes for the observation of photon correlation functions in circuit QED with linear detectors, Phys. Rev. A **82**, 043804 (2010).

[2] O. Gamel and D. F. V. James, Time-averaged quantum dynamics and the validity of the effective Hamiltonian model, Phys. Rev. A **82**, 052106 (2010).

[3] O. D. Stefano, R. Stassi, L. Garziano, A. F. Kockum, S. Savasta, and F. Nori, Feynman-diagrams approach to the quantum Rabi model for ultrastrong cavity QED: Stimulated emission and reabsorption of virtual particles dressing a physical excitation, New J. Phys. **19**, 053010 (2017).

[4] S. Masuda, T. Ishikawa, Y. Matsuzaki, and S. Kawabata, Controls of a superconducting quantum parametron under a strong pump field, Sci. Rep. **11**, 11459 (2021).

[5] A. Petrescu, M. Malekakhlagh, and H. E. Türeci, Lifetime renormalization of driven weakly anharmonic superconducting qubits. II. The readout problem, Phys. Rev. B **101**, 134510 (2020).

[6] See Supplemental Material at http://link.aps.org/supplemental/10.1103/PhysRevApplied.23.054042 for details on additional derivations and numerical results.

[7] W. Fan and H. E. Türeci, Model order reduction for open quantum systems based on measurement-adapted time-coarse graining, arXiv preprint, arXiv:2410.23116.

[8] J. Braumüller, M. Marthaler, A. Schneider, A. Stehli, H. Rotzinger, M. Weides, and A. Ustinov, Analog quantum simulation of the Rabi model in the ultra-strong coupling regime, Nat. Commun. **8**, 779 (2017).

[9] J. Casanova, G. Romero, I. Lizuain, J. J. García-Ripoll, and E. Solano, Deep strong coupling regime of the Jaynes–Cummings model, Phys. Rev. Lett. **105**, 263603 (2010).

[10] S. Ashhab and F. Nori, Qubit-oscillator systems in the ultrastrong-coupling regime and their potential for preparing nonclassical states, Phys. Rev. A **81**, 042311 (2010).

[11] J. Casanova, G. Romero, I. Lizuain, J. J. García-Ripoll, and E. Solano, Deep strong coupling regime of the Jaynes–Cummings model, Phys. Rev. Lett. **105**, 263603 (2010).

[12] Y. Wang and J. Y. Haw, Bridging the gap between the Jaynes–Cummings and Rabi models using an intermediate rotating wave approximation, Phys. Lett. A **379**, 779 (2015).

[13] M. Amniat-Talab, S. Guérin, and H. R. Jauslin, Quantum averaging and resonances: Two-level atom in a one-mode quantized field, J. Math. Phys. **46**, 042311 (2005).

[14] J. Venkatraman, X. Xiao, R. G. Cortiñas, A. Eickbusch, and M. H. Devoret, Static effective Hamiltonian of a rapidly driven nonlinear system, Phys. Rev. Lett. **129**, 100601 (2022).

[15] M. Krack and J. Gross, *Harmonic Balance for Nonlinear Vibration Problems*, Mathematical Engineering (Springer International Publishing, Cham, 2019).

[16] J. Košata, J. Del Pino, T. L. Heugel, and O. Zilberberg, HarmonicBalance.jl: A Julia suite for nonlinear dynamics using harmonic balance, SciPost Phys. Codebases **6**, 039 (2022).

[17] L. L. Buishvili and M. G. Menabde, Higher approximations in the theory of the average Hamiltonian, Theor. Math. Phys. **46**, 166 (1981).

[18] N. M. Krylov and N. N. Bogolyubov, *Introduction to Non-linear Mechanics* (Princeton University, Princeton, 1947).

[19] S. Rahav, I. Gilary, and S. Fishman, Effective Hamiltonians for periodically driven systems, Phys. Rev. A **68**, 013820 (2003).

[20] J. Cary, Lie transform perturbation theory for Hamiltonian systems, Phys. Rep. **79**, 129 (1981).

[21] T. P. Grozdanov and M. J. Raković, Quantum system driven by rapidly varying periodic perturbation, Phys. Rev. A **38**, 1739 (1988).

[22] Z. Xiao, E. Doucet, T. Noh, L. Ranzani, R. Simmonds, L. Govia, and A. Kamal, Perturbative diagonalization for time-dependent strong interactions, Phys. Rev. Appl. **18**, 024009 (2022).

[23] J. H. Shirley, Solution of the Schrödinger equation with a Hamiltonian periodic in time, Phys. Rev. **138**, B979 (1965).

[24] R. M. Wilcox, Exponential operators and parameter differentiation in quantum physics, J. Math. Phys. **8**, 962 (1967).

[25] F. Casas, J. A. Oteo, and J. Ros, Floquet theory: Exponential perturbative treatment, J. Phys. A: Math. Gen. **34**, 3379 (2001).

[26] A. Eckardt and E. Anisimovas, High-frequency approximation for periodically driven quantum systems from a Floquet-space perspective, New J. Phys. **17**, 093039 (2015).

[27] C. Müller and T. M. Stace, Deriving Lindblad master equations with Keldysh diagrams: Correlated gain and loss in higher order perturbation theory, Phys. Rev. A **95**, 013847 (2017).

[28] C.-W. Lee, C. Noh, and J. Kim, Effective formalism for open-quantum-system dynamics: Time-coarse-graining approach, Phys. Rev. A **97**, 012102 (2018).

[29] M. Mirrahimi and P. Rouchon, Dynamics and control of open quantum systems *Lect. Notes* (2015), https://cas.mines-paristech.fr/∼rouchon/LIASFMA/LectureNotes20211202.pdf

[30] D. Chruściński and S. Pascazio, A brief history of the GKLS equation, Open Syst. Inf. Dyn. **24**, 1740001 (2017).

[31] D. Manzano, A short introduction to the Lindblad master equation, AIP Adv. **10**, 025106 (2020).
[32] J. D. Cresser and C. Facer, Coarse-graining in the derivation of Markovian master equations and its significance in quantum thermodynamics, arXiv preprint, arXiv:1710.09939.
[33] D. F. James and J. Jerke, Effective Hamiltonian theory and its applications in quantum information, Can. J. Phys. **85**, 625 (2007).
[34] C. Majenz, T. Albash, H.-P. Breuer, and D. A. Lidar, Coarse graining can beat the rotating-wave approximation in quantum Markovian master equations, Phys. Rev. A **88**, 012103 (2013).
[35] G. Lindblad, On the generators of quantum dynamical semigroups, Commun. Math. Phys. **48**, 119 (1976).
[36] V. Gorini, A. Kossakowski, and E. C. G. Sudarshan, Completely positive dynamical semigroups of N-level systems, J. Math. Phys. **17**, 821 (1976).
[37] P. Pechukas, Reduced dynamics need not be completely positive, Phys. Rev. Lett. **73**, 1060 (1994).
[38] R. Alicki, Comment on "Reduced dynamics need not be completely positive", Phys. Rev. Lett. **75**, 3020 (1995).
[39] P. Pechukas, Pechukas replies:, Phys. Rev. Lett. **75**, 3021 (1995).
[40] A. Grimm, N. E. Frattini, S. Puri, S. O. Mundhada, S. Touzard, M. Mirrahimi, S. M. Girvin, S. Shankar, and M. H. Devoret, Stabilization and operation of a Kerr-cat qubit, Nature **584**, 205 (2020).
[41] M. Bukov, M. Kolodrubetz, and A. Polkovnikov, Schrieffer-Wolff transformation for periodically driven systems: Strongly correlated systems with artificial gauge fields, Phys. Rev. Lett. **116**, 125301 (2016).
[42] L. Bello, W. Fan, A. Gandotra, and H. Türeci, GitHub, 2022, https://github.com/leonbello/quantumgraining.jl.